Journal of Hazardous Materials 197 (2011) 389–396

Contents lists available at SciVerse ScienceDirect

Journal of Hazardous Materials

journal homepage: www.elsevier.com/locate/jhazmat

Adsorption behavior of multi-walled carbon nanotubes for the removal of olaquindox from aqueous solutions

Lei Zhang*, Tianci Xu, Xueyan Liu, Yunyu Zhang, Hongjing Jin

College of Chemistry, Liaoning University, 66 Chongshan Middle Road, Shenyang110036, People's Republic of China

ARTICLE INFO

Article history:
Received 10 July 2011
Received in revised form 3 September 2011
Accepted 29 September 2011
Available online 5 October 2011

Keywords:
Olaquindox
Multi-walled carbon nanotubes
Adsorption
Kinetics
Thermodynamics

ABSTRACT

Multi-walled carbon nanotubes (MWCNT) were employed for the sorption of olaquindox (OLA) from aqueous solution. A detailed study of the adsorption process was performed by varying pH, ionic strength, sorbent amount, sorption time and temperature. The adsorption mechanism is probably the non-electrostatic π–π dispersion interaction and hydrophobic interaction between OLA and MWCNT. The adsorption efficiency could reach 99.7%, suggesting that MWCNT is excellent adsorbents for effective OLA removal from water. OLA adsorption kinetics were found to be very fast and equilibrium was reached within 2.0 min following the pseudo-second-order model with observed rate constants (k) of 0.169–1.048 g mg^{-1} min^{-1} (at varied temperatures). The overall rate process appeared to be influenced by both external mass transfer and intraparticle diffusion, but mainly governed by intraparticle diffusion. A rapid initial adsorption behavior occurred within a short period of time in this adsorption system. The sorption data could be well interpreted by the Langmuir model with the maximum adsorption capacity of 133.156 mg g^{-1} (293 K) of OLA on MWCNT. The mean energy of adsorption was calculated to be 0.124 kJ mol^{-1} (293 K) from the Dubinin–Radushkevich adsorption isotherm. Moreover, the thermodynamic parameters showed the spontaneous, exothermic and physical nature of the adsorption process.

© 2011 Elsevier B.V. All rights reserved.

1. Introduction

Olaquindox (OLA; 2-(*N*-2-hydroxyethylcarbamonyl)-3-methylquinoxaline-N^1,N^4-dioxide) is one of the quinoxaline 1,4-dioxide derivatives which are a group of synthetic antibacterial agents. It is a well known feed additive and was widely used to promote growth, to improve feed efficiency, and to control swine dysentery and bacterial enteritis in the swine industry during the last century. However, large numbers of studies demonstrated its severe phototoxicity, mutagenicity, genotoxicity and carcinogenicity [1–11]. Therefore, the Commission of the European Community forbad the usage of olaquindox as animal growth promoter in 1998 [12]. But OLA is still broadly used as feed additive for swine, poultry and aquatic products in some regions of the world, which has caused wide public concern. In the fish feeding process, feed contained OLA is scattered to rearing pond where OLA accumulated, which brings an amount of OLA into environment. Besides, OLA in aquatic animals will be excreted into water with the metabolism of aquatic organisms. All of these will have potential negative effects on the environment. Consequently the removal of olaquindox from environmental samples is of great significance. To the best of our knowledge, there is no report of the removal of OLA from water by any sorbent.

Carbon nanotubes (CNTs), ever since their discovery, have attracted extensive attention due to their unique physicochemical and electrical properties. CNTs, which are considered to be extremely superior adsorbents due to their high specific surface area and large micropore volume, have been utilized for the sorption of a number of different organic compounds and inorganic ions [13–19], since the first report of their successful removal of dioxin [20]. However, very little is known about the kinetic and thermodynamic characteristics of OLA adsorption on CNTs.

In this work, multi-walled carbon nanotubes (MWCNT) were chosen as sorbent which showed much higher adsorption percentage for OLA than general sorbents, and the adsorption kinetics, isotherms and thermodynamics of OLA on MWCNT were systematically studied for the first time. The aim of this work was to understand the interaction between OLA and MWCNT and to optimize conditions for maximum removal of OLA from aqueous solutions on MWCNT. This information will be useful when designing and operating OLA removal systems based on varying local water qualities. Besides, in our further study, MWCNT will be

* Corresponding author. Tel.: +86 24 62207809; fax: +86 24 62202380.
E-mail address: zhanglei63@126.com (L. Zhang).

0304-3894/$ – see front matter © 2011 Elsevier B.V. All rights reserved.
doi:10.1016/j.jhazmat.2011.09.100

used to make an electrochemical sensor of OLA, so this research of MWCNT adsorption behavior for OLA will provide a theoretical basis for on-line monitoring of OLA.

2. Materials and methods

2.1. Apparatus

The HPLC system Agilent 1100 (Agilent Technologies Co. Ltd., USA) was used for the determination of OLA. UV-Vis-NIR Cary 5000 (VARIAN Co., US) was used to record the absorption spectra of OLA for the selection of sorbents. A S-3C Model pH meter (Shanghai Precision Scientific Instrument Co., China) was used for measuring the pH of solutions. A model DF-101B thermostatic magnetic stirrer (Gongyi Yingyu Yuhua Instrument Co., China) was used to stir the solution contained OLA and CNTs, and to control the solution temperature with the thermostatic bath equipped. A model TDL80-2B centrifugal machine (Shanghai Anting Scientific Instrument Co., China) was used to separate solid/liquid phases after adsorption. The morphology of CNTs was determined by transmission electron microscopy (TEM, Hitachi 800) operated at 200 kV. TEM samples were prepared using CNTs dispersed in acetone. A drop of the sample was placed onto a lacy carbon film supported by a Cu grid, and then it was observed. The functional groups of MWCNT surface and OLA were detected by AVATAR 330 Fourier transform infrared spectroscopy (FTIR) (NICOLET Co., USA). The thermal stability of MWCNT was determined by a TGA/SDTA 851^e thermogravimetric analyzer (Mettler-Toledo, Switzerland) at a heating rate of 20 °C/min from 35 °C to 1000 °C under 20 mL min^{-1} Ar flow.

2.2. Chemicals

Six CNTs (95% purity) (pristine [MWCNT, Short–MWCNT], hydroxyl functionalized [MWCNT–OH, Short–MWCNT–OH] and carboxyl functionalized [MWCNT–COOH, Short–MWCNT–COOH]) were purchased from Chengdu Organic Chemicals Co., Ltd, Chinese Academy of Sciences. Each of the six CNTs has a specific surface area above 500 m^2 g^{-1} and an outer diameter below 8 nm. Pore distributions (pore volume with pore diameter in parentheses) of MWCNT used as sorbent throughout the experiment are as follows: 0.085 m^3 g^{-1} (0–20 nm), 1.839 m^3 g^{-1} (20–50 nm). All these physical parameters of CNTs were provided by the manufacturer. Nano-particles (nano-SiO_2, nano-γ-Al_2O_3 and nano-TiO_2) were purchased from Zhoushanmingri Nanometer Material Co., China. Carbonaceous materials (active carbon, graphene and bamboo carbon) were provided by Liaoning Medical Company, China.

The analytical standard OLA ($C_{12}H_{13}N_3O_4$; MW 263.25; solubility at 25 °C: 5 mg mL^{-1} in water; CAS no. 23696-28-8; 98.4% purity) was purchased from China Institute of Veterinary Drug Control (Beijing, China), and its molecular structure is as follows:

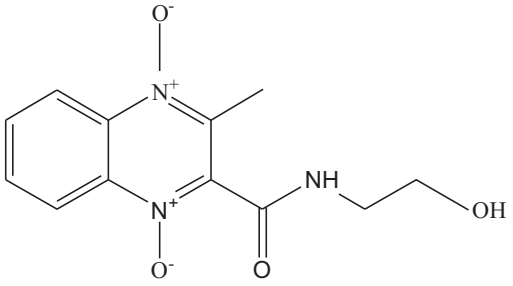

HPLC grade methanol was purchased from Fisher Scientific (Fair Lawn, NJ 07410, USA). All other chemicals were of analytical reagent grade or better and purchased from Shenyang Chemical Company, China. Deionized water used throughout experiments was purified using a Sartorius Arium 611 system (Sartorius, Göttingen, Germany).

A 1.0 mg mL^{-1} standard stock solution of OLA was prepared by dissolving 254.1 mg OLA in deionized water and diluting to the mark in a 250 mL brown volumetric flask, and was kept in the dark below 4 °C.

Table 1
Adsorption efficiency for OLA on general carbon materials and nano-particles (C_{OLA}: 40.0 mg L^{-1}; at OLA natural pH 5.3; Temp. 20 ± 0.1 °C; stirring for 1.5 h).

Sorbents	Optimum amount (mg)	*Ads.%*
Actived carbon	70.0	10.5
Graphene	50.0	4.5
Bamboo carbon	40.0	4.0
Nano-SiO_2 (20 nm)	20.0	1.2
Nano-TiO_2 (anatase type, 10–15 nm)	20.0	1.2
Nano-Al_2O_3 (γ, 10 nm)	20.0	0.9
Nano-TiO_2 (rutile type, 10–15 nm)	10.0	0.0

2.3. General adsorption procedure

The adsorption experiments were carried out using a series of 50 mL flasks containing 10.0 mg MWCNT and 25 mL of 40.0 mg L^{-1} OLA solution. If necessary, the pH of the solutions was adjusted by adding H_3PO_4 or NaOH solution, and the ionic strength of the solutions was adjusted by dissolving different amount of NaCl solids in them before the addition of MWCNT. After stirring at a constant rate at 293 K for 2.0 min, the solid/liquid phases were separated by centrifuging at 5000 rpm for 5 min. Then the concentration of OLA in suspensions was determined by the HPLC system Agilent 1100 equipped with an autoinjector, a diode array detector, and a SB-C_{18} reversed-phase column (150 mm × 4.6 mm i.d., 5 μm). The column temperature was set at 35 °C, and the injection volume was 20 μL. The mobile phase was 15/85 (volume ratio) methanol/water, and the flow rate was 1.0 mL min^{-1}. The detection and reference wavelengths were 380 and 500 nm, respectively. The retention time of OLA was 4.382 min.

The adsorption percentage (*Ads.%*) was calculated based on the following equation:

$$Ads.\% = \frac{C_i - C_a}{C_i} \times 100 \quad (1)$$

where C_i and C_a are the initial and the final concentration of OLA in solution phase, respectively.

Kinetic experiments were performed using a series of 50 mL flasks containing 50.0 mg MWCNT and 25 mL of 90.0 mg L^{-1} OLA solution in a temperature range of 293–333 K. On regular time intervals, suitable aliquots were taken whereupon the OLA concentration was determined. The rate constants were calculated using the conventional rate expression. An experiment without MWCNT was carried out confirming that no adsorption occurred on the container wall or the magnet in solution.

Adsorption isotherm studies were carried out with initial concentrations of OLA varying between 8.0 and 300.0 mg L^{-1}, the amount of sorbent was kept constant (10.0 mg) and the experimental temperatures were controlled at 293, 313 and 333 K, respectively. The thermodynamic parameters for the adsorption process were determined at each temperature.

3. Results and discussion

3.1. Selection of sorbents

Seven general sorbents (listed in Table 1) were chosen to test their adsorbability of OLA. In order to make their adsorption efficiency for OLA as high as possible, the adsorption conditions

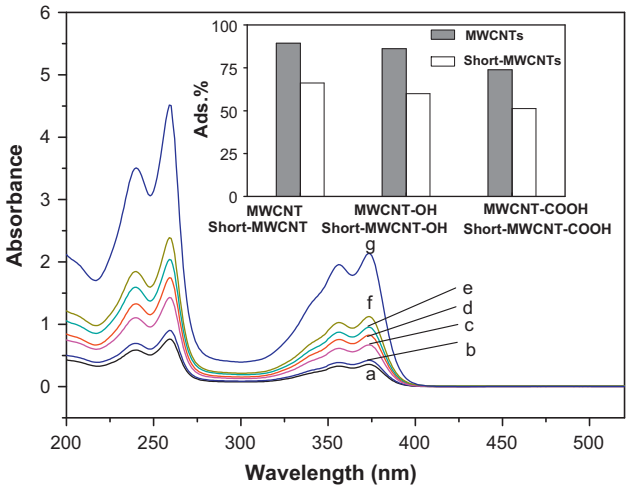

Fig. 1. Effect of different CNTs on adsorption behavior of OLA (10.0 mg CNTs; pH 5.3; C_{OLA}: 40.0 mg L^{-1}; temp. 20 ± 0.1 °C); a: MWCNT; b: MWCNT–OH; c: MWCNT–COOH; d: Short–MWCNT; e: Short–MWCNT–OH; f: Short–MWCNT–COOH; g: original solution; inset image: the corresponding adsorption efficiency for OLA on different CNTs.

(solution pH, sorbent amount) of each sorbent were optimized. As could be seen from Table 1 that OLA could not be effectively adsorbed by general carbonaceous materials and nano-particles, so a highly effective sorbent is needed.

The adsorption of OLA on different types of CNTs was studied, and the UV–vis absorption spectrogram of OLA solutions was shown in Fig. 1. It could be seen that the adsorption percentages for OLA on CNTs were much higher than that on general sorbents (Table 1).

Usually, adsorbability depends on adsorbent's characteristics: texture (surface area, pore distributions), surface chemistry (surface functional groups), and mineral matter content. It also depends on adsorbate's characteristics: molecular weight, polarity, pK_a, molecular size and functional groups. CNTs with high specific surface area and large micropore volume are more appropriate for the adsorption of organic compounds, compared to the general carbonaceous materials and nano-particles.

Moreover, MWCNTs (length 10–30 μm) showed higher adsorption efficiency for OLA than Short–MWCNTs (length 0.5–2 μm), and the adsorption efficiency for OLA on MWCNTs followed the order MWCNT > MWCNT–OH > MWCNT–COOH. Therefore, MWCNT was used as sorbents for OLA in the experiment.

Due to strong van der Waals interactions, MWCNT adhere to each other and form bundles, and the space between the bundles can be considered as pores, which provided more adsorption sites than Short–MWCNT. Therefore, MWCNT showed higher adsorption efficiency than Short–MWCNT. Moreover, functional groups of MWCNT may increase diffusional resistance [21–23]. And water molecules could form H-bonds with functional groups on MWCNT, which will form a three-dimensional cluster that either covers the sorption sites nearby or blocks the access of OLA molecules to the sorption sites. In addition, the stronger the functional groups' polarity is, the easier the formation of H-bonds between water molecules and functional groups will be, so the negative effects of H-bonds on adsorption caused by –COOH of MWCNT were more obvious than that caused by –OH in this study.

3.2. Characterizations of CNTs and CNTs-OLA

Fig. 2A and B displays the TEM images of MWCNT and Short–MWCNT, respectively. A large amount of pores appeared within MWCNT. The process of forming bundles or pores creates

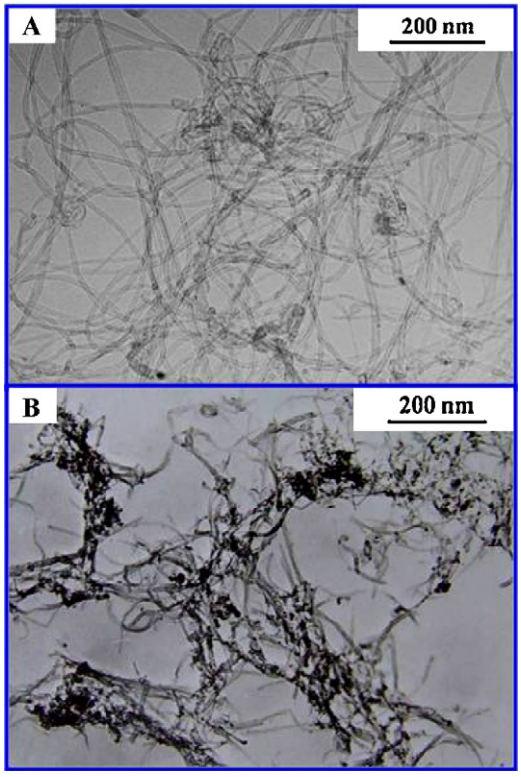

Fig. 2. Transmission electron microscope (TEM) images of MWCNT (A) and Short–MWCNT (B).

lots of adsorption sites, such as the interstitial channel, the external groove, and partial coating of the external surface by nanometer-thick layered carbon [24]. All of these sites contribute to overall adsorption.

It was found from the FTIR spectra that MWCNT after adsorption (MWCNT-OLA) showed some apparent characteristic bands of OLA which were N–H (3434 cm^{-1}), C–H (2923 cm^{-1}), C=O (1655 cm^{-1}) and =C–H (1079 cm^{-1}), while MWCNT before adsorption displayed no significant bands.

The TG curve of MWCNT-OLA showed an obvious 9.1% weight loss caused by the thermal decomposition of OLA adsorbed on MWCNT, compared with the TG curve of MWCNT before adsorption.

3.3. Effect of pH

25 mL of solutions with different concentrations (20.0–60.0 mg L^{-1}) of OLA were applied to test the sorption behavior at different pH values. The obtained results indicated that there was no observable effect on the adsorption of OLA on MWCNT with an increase of pH from 3.0 to 11.0, and when the concentration of OLA was less than 40 mg L^{-1}, the adsorption percentage of OLA was found to be above 88%. In general, the natural pH of OLA solution was close to 5.3. In this work the OLA solution without adjusting pH was popularly adopted.

The variation in pH can not only affect the protonation–deprotonation transition of functional groups on CNTs [25,26], but also result in a change in chemical speciation for ionizable organic compounds [26,27]. OLA is amphoteric due to the presence of hydroxyl and amino, so it is characterized by 2 pK_a values. The two predicted pK_a values of OLA are 1.92 ± 0.30 and 13.75 ± 0.10, respectively, which are from SciFinder Scholar and calculated using Advanced Chemistry Development (ACD/Labs) Software V11.02 (© 1994–2011 ACD/Labs).

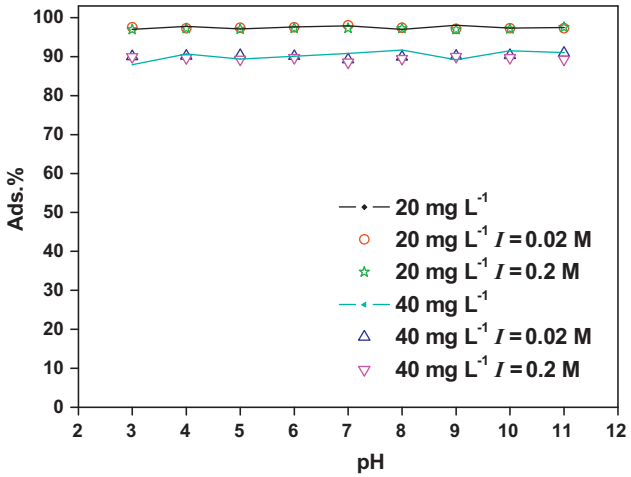

Fig. 3. Effect of ionic strength on the adsorption efficiency of OLA on MWCNT at different initial OLA concentrations (10.0 mg MWCNT; temp. 20 ± 0.1 °C).

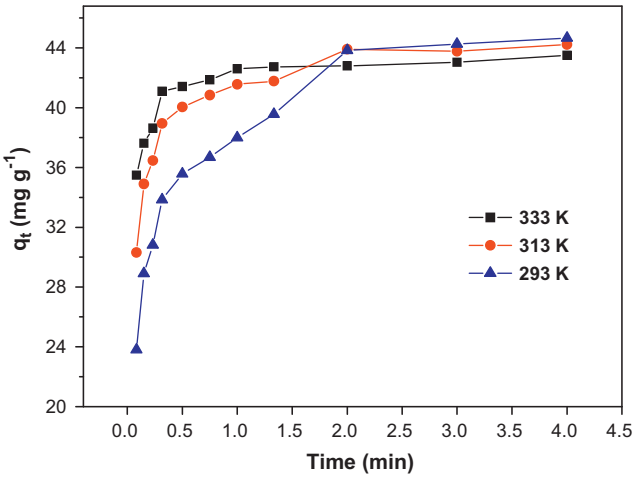

Fig. 4. Adsorption capacity of OLA on MWCNT versus time at different temperatures (50.0 mg MWCNT; C_{OLA}: 90.0 mg L^{-1}).

The amphoteric compounds usually have four chemical species in solution [28]. When solution pH is below 1.92, OLA will exist as a cation ($OLAH_3^+$) due to the protonation of the amino. When solution pH is above 13.75, OLA will exist as an anion ($OLAH^-$) due to the loss of proton from the hydroxyl. At pH between 1.92 and 13.75, OLA will exist either as a neutral molecule ($OLAH_2^0$) or as a zwitterion ($OLA\,H_2^{\pm}$). On this condition, nearly all of OLA molecules carry no net electrical charge, which makes them hardly have electrostatic attraction or repulsion with MWCNT, so the increase of pH from 3.0 to 11.0 had no significant effect on the adsorptive affinity of OLA in the experiment. Consequently, the adsorption mechanism is probably the non-electrostatic π–π dispersion interaction between bulk π systems on MWCNT surface and OLA molecules contained both benzene rings and double bonds (C=C; C=O), or hydrophobic interaction between MWCNT and OLA [29,30].

3.4. Effect of ionic strength

OLA adsorption data under two ionic strengths (I; 0.02 and 0.2 M as NaCl) and two initial OLA concentrations (20.0 and 40.0 mg L^{-1}) are given in Fig. 3. In the entire experimental pH range, the OLA adsorption data for each concentration under two ionic strengths overlapped, indicating that ionic strength did not impact the adsorption of OLA onto MWCNT. Furthermore, this result again confirmed that the surface electrostatic effect had no influence on the overall adsorption of OLA on MWCNT. In this experiment, the OLA solution without adjusting ionic strength was adopted.

3.5. Effect of the amount of MWCNT

In order to attain the optimal amount of MWCNT for the adsorption of OLA, the adsorption experiments were carried out by adding 10.0–100.0 mg of MWCNT to a series of 25 mL 40.0 mg L^{-1} OLA solutions. It was found that the adsorption percentage increased with the increasing amount of MWCNT, and when the amount exceeded 50.0 mg, the adsorption percentage reached 99.7% with no obvious change. Therefore, the MWCNT amount 50.0 mg was selected for the adsorption of OLA.

3.6. Adsorption kinetics and rate-controlling mechanism

Fig. 4 depicts the variation of adsorption capacity with adsorption time at different temperatures. The obtained curves reflected that the adsorption capacity increased until equilibrium was rapidly attained around 2.0 min.

In order to investigate the adsorption process of OLA on MWCNT, pseudo-second-order, Weber–Morris and Boyd models were used.

3.6.1. Pseudo-second-order model

The pseudo-second-order model is represented as [31]:

$$\frac{t}{q_t} = \frac{1}{kq_e^2} + \frac{t}{q_e} \quad (2)$$

where q_e and q_t are the amounts of OLA adsorbed on the sorbent (mg g^{-1}) at equilibrium and at time t, respectively, and k is the rate constant of the second-order adsorption (g mg^{-1} min^{-1}). The straight-line plots of t/q_t versus t have been tested to obtain rate parameters.

The second-order rate constants were used to calculate the initial sorption rate h (mg g^{-1} min^{-1}) [32], given by

$$h = kq_e^2 \quad (3)$$

The pseudo-second-order model adequately described the kinetic data at 95% confidence level. The results of the kinetic parameters and the calculated initial sorption rate values are listed in Table 2. Based on the correlation coefficients ($r \geq 0.999$) the adsorption of OLA could be well described by the pseudo-second-order model. The rate constant (k) was quite large, indicating that the adsorption of OLA on MWCNT was a fast process. And the initial adsorption rate increased with the increasing temperature in a given adsorption system.

3.6.2. Weber–Morris kinetic model

If the movement of adsorbate from the bulk liquid to the liquid film surrounding the adsorbent is ignored, the adsorption process in porous solids can be separated into three stages as follows: (1) external mass transfer of adsorbate across the liquid film to the adsorbent exterior surface, which is also called film diffusion (or boundary layer diffusion or outer diffusion); (2) transport of adsorbate from the adsorbent exterior surface to the pores or capillaries of the adsorbent internal structure, which is called intraparticle diffusion (or inner diffusion); (3) the adsorbate is adsorbed onto the

Table 2
Kinetic parameters of pseudo-second-order model fitting for OLA adsorption on MWCNT at different temperatures.

T (K)	k (g mg^{-1} min^{-1})	q_e (mg g^{-1})	h (mg g^{-1} min^{-1})	r
293	0.169	45.662	352.113	0.999
313	0.425	44.484	840.336	1
333	1.048	43.346	1969.019	1

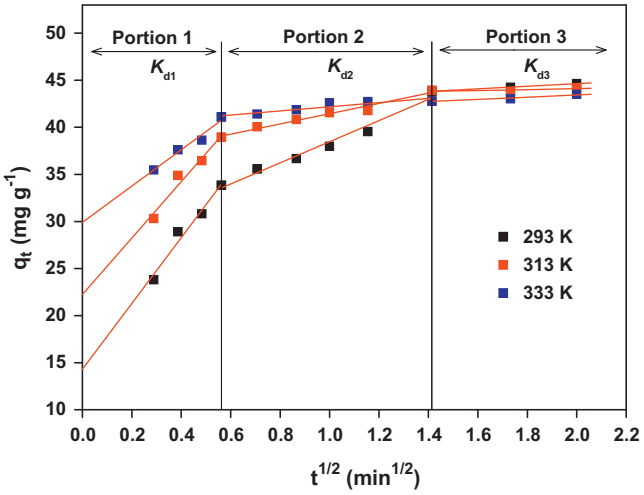

Fig. 5. Weber–Morris plots for kinetic modeling of OLA adsorbed onto MWCNT at different temperatures.

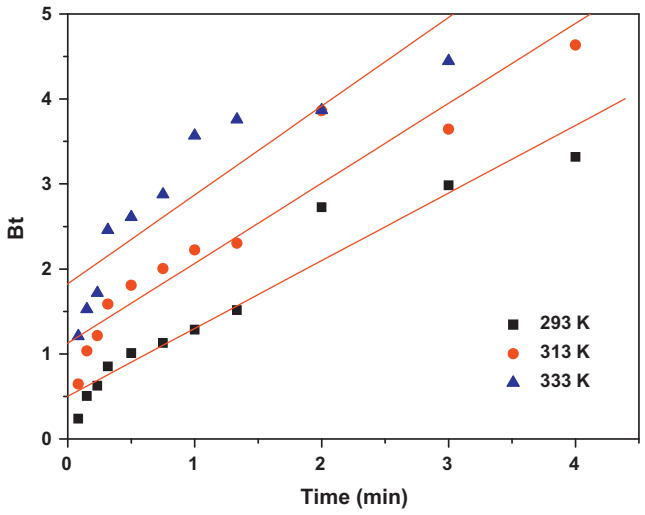

Fig. 6. Plots of *Bt* versus *t* for the adsorption of OLA on MWCNT at different temperatures.

active sites in inner and outer surface of adsorbent [33–35]. The third step is considered to be very fast and thus cannot be treated as rate limiting step. Generally, the adsorption rate is controlled by outer diffusion or inner diffusion or both.

In order to determine the actual rate-controlling step involved in the OLA sorption process, Weber–Morris equation was applied [36]:

$$q_t = K_d t^{1/2} + L \tag{4}$$

K_d is the intraparticle diffusion rate constant (mg g^{-1} min$^{-1/2}$). Values of L (mg g^{-1}) give an idea about the thickness of the boundary layer, i.e., the larger the intercept, the greater the boundary layer effect will be [37,38]. Plots of q_t against $t^{1/2}$ are shown in Fig. 5, and the corresponding kinetic parameters are listed in Table 3.

Piecewise linear regression of data showed that at all the tested temperatures, q_t versus $t^{1/2}$ plots had three distinct regions. The first linear portion included the sorption period of 0–19 s, which represented external mass transfer. The second linear portion included the sorption period of 19–120 s, representing intraparticle diffusion. The third linear portion included the time period of 120–240 s, which indicated adsorption–desorption equilibrium [39,40].

It was also observed that the plots did not pass through the origin, suggesting that the intraparticle diffusion is not the sole rate-controlling step [32] and the external mass transfer is also significant in the rate-controlling step due to the large intercepts of the second linear portion of the plots [41]. However, the ratio of the time taken by external mass transfer to intraparticle diffusion was about 1:5. So the overall adsorption process was jointly controlled by external mass transfer and intraparticle diffusion, and intraparticle diffusion was predominated over the external mass transfer.

It should be pointed out that the intercepts of the first linear portion of the plots are positive and large, indicating that rapid initial adsorption occurred within a short period of time. Wu et al. [42] defined an initial adsorption factor for Weber–Morris model (R_i) which is calculated from the following equation:

$$\frac{q_t}{q_{\text{ref}}} = 1 - R_i \left[1 \left(\frac{t}{t_{\text{ref}}}\right)^{1/2}\right] \tag{5}$$

where t_{ref} is the longest time in adsorption process (min) and q_{ref} is the amount of OLA adsorbed on the MWCNT (mg g^{-1}) at time $t = t_{\text{ref}}$, and $R_i = k_d t^{1/2}/q_{\text{ref}}$. The dimensionless parameter R_i is obtained by plotting q_t/q_{ref} versus t/t_{ref} and from nonlinear analysis of data. The percentage that the initial adsorption has already reached (*Ini.%*) can be calculated as:

$$Ini.\% = (1 - R_i) \times 100 \tag{6}$$

It was found that at 293 K the initial adsorption had already reached 49.9% ($R_i = 0.501$, $r^2 = 0.875$) and the values of *Ini.%* increased with the increase of temperature ($R_i = 0.300$, $r^2 = 0.745$, *Ini.%* = 70.0, at 313 K; $R_i = 0.174$, $r^2 = 0.667$, *Ini.%* = 82.6, at 333 K), which agrees well with the obtained rapid initial adsorption rate *h* (Table 2), suggesting that MWCNT has great adsorptive affinity for OLA.

3.6.3. Boyd model

Adsorption kinetic data was further analyzed by Boyd model [43,44]:

$$Bt = -\ln\left(1 - \frac{q_t}{q_e}\right) - 0.4977 \tag{7}$$

where q_t and q_e are the amounts of OLA adsorbed on MWCNT (mg g^{-1}) at time t (min) and at equilibrium time (min), respectively; $B = \pi^2 D_i/r^2$ (D_i is the effective diffusion coefficient of adsorbate and r is the radius of adsorbent particles assumed to be spherical).

The calculated *Bt* values were plotted against time *t* as shown in Fig. 6. The linearity of the plots will provide useful information to distinguish between external mass transfer and intraparticle diffusion controlled mechanism of adsorption [44,45]. The plots in Fig. 6 did not pass through the origin, confirming the involvement

Table 3
Kinetic parameters calculated from Weber–Morris kinetic model for OLA adsorption on MWCNT at different temperatures.

T (K)	K_{d1} (mg g^{-1} min$^{-1/2}$)	K_{d2} (mg g^{-1} min$^{-1/2}$)	K_{d3} (mg g^{-1} min$^{-1/2}$)	L_1	L_2	L_3	r_1	r_2	r_3
293	34.971	11.225	1.387	14.288	27.243	41.872	0.984	0.988	0.999
313	30.028	5.422	0.492	22.230	36.026	43.128	0.981	0.986	0.635
333	19.321	2.217	1.187	29.888	39.974	41.075	0.984	0.934	0.974

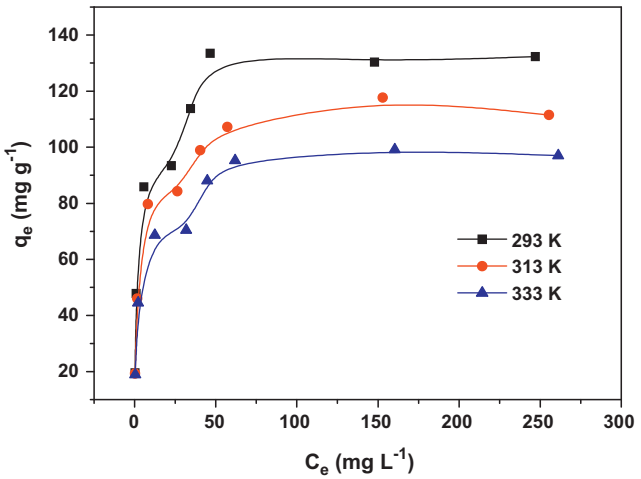

Fig. 7. Isotherm of OLA adsorption on MWCNT at different temperatures (10.0 mg of MWCNT; the initial OLA concentration range was 8.0–300.0 mg L^{-1}).

of external mass transfer in the entire adsorption process [46]. However, the plots were not straight lines, indicating that external mass transfer shows a relative weak rate control for OLA adsorption onto MWCNT. This result again confirms the rate-controlling mechanism of adsorption stated in Weber–Morris kinetic model studies.

3.7. Adsorption isotherms

Adsorption isotherms describe how solutes interact with sorbents. The equilibrium adsorption amount of OLA on MWCNT as a function of the equilibrium concentration of OLA is depicted in Fig. 7. An increased adsorption is observed for OLA until saturation is attained.

Equilibrium sorption isotherms are often described by the Langmuir model:

$$\frac{C_e}{q_e} = \frac{C_e}{q_m} + \frac{1}{bq_m} \tag{8}$$

where q_m is the maximum monolayer adsorption (mg g^{-1}), C_e is the equilibrium concentration of OLA (mg L^{-1}), q_e is the amount of OLA adsorbed per unit weight of MWCNT at equilibrium concentration (mg g^{-1}) and b is the Langmuir constant related to the affinity of binding sites (L mg^{-1}). The corresponding Langmuir isotherm constants were determined from the plots of C_e/q_e against C_e at 293, 313 and 333 K.

The obtained isothermal constants and the correlation coefficients are presented in Table 4. Langmuir isotherm model was statistically significant at a 95% confidence level. It was found that the adsorption of OLA on MWCNT correlated well with the Langmuir equation under the studied concentration range according to the correlation coefficient r ($r > 0.99$). The maximum adsorption capacity of OLA on MWCNT was 133.156, 120.192, 101.937 mg g^{-1} at 293, 313 and 333 K, respectively.

The shape of the isotherm has been discussed with the aim to predict whether an adsorption system is favorable or unfavorable [47]. The essential feature of the Langmuir isotherms can be expressed by means of 'R_L', a dimensionless constant referred to as the separation factor or equilibrium parameter. R_L is calculated using the following equation:

$$R_L = \frac{1}{1 + bC_i} \tag{9}$$

where C_i is the initial OLA concentration (mg L^{-1}) and b is the Langmuir adsorption equilibrium constant (L mg^{-1}). The calculated R_L values are listed in Table 4. In the present investigation, the equilibrium parameter R_L was found to be in the range of 0–1, hence the sorption process was quite favorable and the adsorbent employed exhibited a good potential for the sorption of OLA.

Finally, the Dubinin–Radushkevich (D–R) isotherm [48] was also tested in its linearized form:

$$\ln\ q_e = \ln q_m - K\varepsilon^2 \tag{10}$$

where q_e and q_m have the same meaning as above, K is the parameter related to the adsorption energy. ε is the adsorption potential, defined by Polanyi as the free energy change required to move a molecule from bulk solution to the adsorption area. The Polanyi potential varies with the concentration according to:

$$\varepsilon = RT\ \ln\left(1 + \frac{1}{C_e}\right) \tag{11}$$

where R is the ideal gas constant and T is temperature (K). A linear correlation was obtained by plotting $\ln q_e$ versus ε^2 ($r_1 = -0.962$ at 293 K; $r_2 = -0.985$ at 313 K; $r_3 = -0.974$ at 333 K), indicating that OLA adsorption also obeys the D–R equation. The adsorption energy for OLA adsorption can be calculated by:

$$E = (-2K)^{-1/2} \tag{12}$$

The values of the adsorption energy were evaluated as 0.124, 0.122 and 0.104 kJ mol^{-1}, at 293, 313 and 333 K, respectively, indicating that the values lie within the energy range of physical adsorption, i.e., <8 kJ mol^{-1} [49].

3.8. Thermodynamic studies

Thermodynamic parameters were calculated from following equations:

$$\Delta G^\circ = -RT \ln K_c \tag{13}$$

where R is the universal gas constant (8.314 J mol^{-1} K^{-1}), T is temperature (K) and K_c is the distribution coefficient. Gibbs free energy change of adsorption (ΔG°) was calculated using $\ln K_c$ values for different temperatures. The K_c value was calculated using following equation [50]:

$$K_c = \frac{q_e}{C_e} \tag{14}$$

where C_e is the equilibrium concentration of OLA; q_e is the amount of OLA adsorbed per unit weight of MWCNT at equilibrium concentration (mg g^{-1}).

The enthalpy change (ΔH°) and entropy change (ΔS°) of adsorption were estimated from the following equation:

$$\ln\ K_c = \frac{\Delta S^\circ}{R} - \frac{\Delta H^\circ}{RT} \tag{15}$$

According to Eq. (15), ΔH° and ΔS° parameters can be calculated from the slope and intercept of the plot of $\ln K_c$ versus $1/T$, respectively.

The thermodynamic parameters were summarized in Table 5. The negative ΔG° showed the spontaneous nature of the sorption process. The negative ΔS° indicated decreased randomness at the solid–liquid interface during sorption of OLA. The value of ΔH° was −10.493 kJ mol^{-1}, which suggested that the adsorption

Table 4
Langmuir constants of OLA adsorption on MWCNT at different temperatures.

T (K)	q_m (mg g^{-1})	b (L mg^{-1})	r	R_L
293	133.156	0.285	0.998	0.017–0.305
313	120.192	0.183	0.998	0.027–0.406
333	101.937	0.171	0.997	0.028–0.422

Table 5
Thermodynamic parameters for the adsorption of OLA on MWCNT.

C_i (mg L^{-1})	ΔH° (kJ mol^{-1})	ΔS° (J mol^{-1} K^{-1})	ΔG° (kJ mol^{-1})		
			293 K	313 K	333 K
80.0	−10.493	−25.955	−2.907	−2.328	−1.874

of OLA onto MWCNT was exothermic and probably a physisorption process caused by van der Waals and hydrophobic forces between MWCNT and OLA, according to the sorption heat of different forces determined by von Oepen et al. [51] (van der Waals force: 4–10 kJ mol^{-1}; Hydrophobic force: about 5 kJ mol^{-1}; Hydrogen bond: 2–40 kJ mol^{-1}; Coordination exchange: about 40 kJ mol^{-1}; Dipole force: 2–29 kJ mol^{-1}; Chemical bond: >60 kJ mol^{-1}). This adsorption mechanism obtained from the analysis of ΔH° value agrees well with those discussed in pH, ionic strength and adsorption energy studies.

4. Conclusion

In this paper, the adsorption behavior of OLA on MWCNT was investigated. Among the seven general sorbents and six types of CNTs, MWCNT showed the highest adsorption efficiency for OLA. The main advantages of the procedure are ease and simple, and can rapidly attain phase equilibration. Besides, MWCNT as sorbent has high adsorption capacity and rate. The experimental results indicate that MWCNT can effectively remove OLA in aqueous solution in wide range of pH 3.0–11.0. The percentage of OLA (40.0 mg L^{-1}) removal by MWCNT can reach 99.7%. Kinetic studies suggest that the equilibrium is achieved within only 2.0 min and the pseudo-second-order model is followed. The overall rate process appears to be influenced by both external mass transfer and intraparticle diffusion, but mainly controlled by the latter. The adsorption isotherms could be well fitted by the Langmuir adsorption isotherm equations with the maximum adsorption capacity of 133.156 mg g^{-1} (293 K) of OLA on MWCNT. The thermodynamic parameters imply that the adsorption is a spontaneous, exothermic and physisorption process. The adsorption mechanism is probably the non-electrostatic π–π dispersion interaction and hydrophobic interaction between OLA and MWCNT. The results obtained in this work suggest that MWCNT has a potential application as adsorbent media for removing OLA from water.

Acknowledgments

This project was supported by National Natural Science Foundation of China (Grant No. 51178212), and Natural Science Foundation of Liaoning Province, China (No. 201102082). The authors also thank their colleagues and other students who participated in this work.

References

[1] Q. He, G. Fang, Y. Wang, Z. Wei, D. Wang, S. Zhou, S. Fan, Z. Yuan, Experimental evaluation of cyadox phototoxicity to Balb/c mouse skin, Photodermatol. Photoimmunol. Photomed. 22 (2006) 100–104.
[2] N.J. Neumann, A. Blotz, G. Wasinska-Kempka, M. Rosenbruch, P. Lehmann, H.J. Ahr, H.W. Vohr, Evaluation of phototoxic and photoallergic potentials of 13 compounds by different in vitro and in vivo methods, J. Photochem. Photobiol. B 79 (2005) 25–34.
[3] H. Belhadjali, M.C. Marguery, F. Journe, F. Giordano-Labadie, H. Lefebvre, J. Bazex, Allergic and photoallergic contact dermatitis to olaquindox in a pig breeder with prolonged photosensitivity, Photodermatol. Photoimmunol. Photomed. 18 (2002) 52–53.
[4] H. Yoshimura, Teratogenic assessment of carbadox in rats, Toxicol. Lett. 129 (2002) 115–118.
[5] L. Hao, Q. Chen, X. Xiao, Molecular mechanism of mutagenesis induced by olaquindox using a shuttle vector pSP189/mammalian cell system, Mutat. Res. 599 (2006) 21–25.
[6] L. Beutin, E. Preller, B. Kowalski, Mutagenicity of quindoxin, its metabolites, and two substituted quinoxaline-di-*N*-oxides, Antimicrob. Agents Chemother. 20 (1981) 336–343.
[7] H. Yoshimura, M. Nakamura, T. Koeda, Mutagenicities of carbadox and olaquindox-growth promoters for pigs, Mutat. Res. 90 (1981) 49–55.
[8] J. Zou, Q. Chen, S. Tang, X. Jin, K. Chen, T. Zhang, X. Xiao, Olaquindox-induced genotoxicity and oxidative DNA damage in human hepatoma G2 (HepG2) cells, Mutat. Res. 676 (2009) 27–33.
[9] Q. Chen, S. Tang, X. Jin, J. Zou, K. Chen, T. Zhang, X. Xiao, Investigation of the genotoxicity of quinocetone, carbadox and olaquindox in vitro using Vero cells, Food Chem. Toxicol. 47 (2009) 328–334.
[10] T. Nunoshiba, H. Nishioka, Genotoxicity of quinoxaline 1,4-dioxide derivatives in *Escherichia coli* and *Salmonella typhimurium*, Mutat. Res. 217 (1989) 203–209.
[11] R. Cihak, V. Srb, Cytogenetic effects of quinoxaline-1,4-dioxide-type growth promoting agents. I. Micronucleus test in rats, Mutat. Res. 116 (1983) 129–135.
[12] Commission of the European Communities, Commission regulation 2788/98, Off. J. Eur. Communities: Legis. L347 (1998) 31–32.
[13] C. Wu, Adsorption of reactive dye onto carbon nanotubes: equilibrium, kinetics and thermodynamics, J. Hazard. Mater. 144 (2007) 93–100.
[14] C. Lu, Y.L. Chung, K.F. Chang, Adsorption of trihalomethanes from water with carbon nanotubes, Water Res. 39 (2005) 1183–1189.
[15] C.J.M. Chin, L.C. Shih, H.J. Tsai, T.K. Liu, Adsorption of *o*-xylene and *p*-xylene from water by SWCNTs, Carbon 45 (2007) 1254–1260.
[16] A. Duran, M. Tuzen, M. Soylak, Preconcentration of some trace elements via using multiwalled carbon nanotubes as solid phase extraction adsorbent, J. Hazard. Mater. 169 (2009) 466–471.
[17] M. Tuzen, K.O. Saygi, C. Usta, M. Soylak, *Pseudomonas aeruginosa* immobilized multiwalled carbon nanotubes as biosorbent for heavy metal ions, Bioresource Technol. 99 (2008) 1563–1570.
[18] M. Tuzen, K.O. Saygi, M. Soylak, Solid phase extraction of heavy metal ions in environmental samples on multiwalled carbon nanotubes, J. Hazard. Mater. 152 (2008) 632–639.
[19] M. Tuzen, M. Soylak, Multiwalled carbon nanotubes for speciation of chromium in environmental samples, J. Hazard. Mater. 147 (2007) 219–225.
[20] R.Q. Long, R.T. Yang, Carbon nanotubes as superior sorbent for dioxin removal, J. Am. Chem. Soc. 123 (2001) 2058–2059.
[21] G. Onyestyak, Z. Otvos, J. Valyon, I. Kiricsi, L.V.C. Rees, Acetylene sorption dynamics in carbon nanotubes, Helv. Chim. Acta 87 (2004) 1508–1514.
[22] H.H. Cho, B.A. Smith, J.D. Wnuk, D.H. Fairbrother, W.P. Ball, Influence of surface oxides on the adsorption of naphthalene onto multiwalled carbon nanotubes, Environ. Sci. Technol. 42 (2008) 2899–2905.
[23] Q. Liao, J. Sun, L. Gao, The adsorption of resorcinol from water using multiwalled carbon nanotubes, Colloid Surf. A 312 (2008) 160–165.
[24] S. Agnihotri, J.P.B. Mota, M. Rostam-Abadi, M.J. Rood, Adsorption site analysis of impurity embedded single-walled carbon nanotube bundles, Carbon 44 (12) (2006) 2376–2383.
[25] S. Zhang, T. Shao, S.S.K. Bekaroglu, T. Karanfil, Adsorption of synthetic organic chemicals by carbon nanotubes: effects of background solution chemistry, Water Res. 44 (2010) 2067–2074.
[26] G.D. Sheng, D.D. Shao, X.M. Ren, X.Q. Wang, J.X. Li, Y.X. Chen, X.K. Wang, Kinetics and thermodynamics of adsorption of ionizable aromatic compounds from aqueous solutions by as-prepared and oxidized multiwalled carbon nanotubes, J. Hazard. Mater. 178 (2010) 505–516.
[27] P. Kulshrestha, R.F. Giese Jr., D.S. Aga, Investigating the molecular interactions of oxytetracycline in clay and organic matter: insights on factors affecting its mobility in soil, Environ. Sci. Technol. 38 (2004) 4097–4105.
[28] J. Hernández-Borrell, M.T. Montero, Calculating microspecies concentration of zwitterion amphoteric compounds: ciprofloxacin as example, J. Chem. Educ. 74 (11) (1997) 1311.
[29] C. Moreno-Castilla, Adsorption of organic molecules from aqueous solutions on carbon materials, Carbon 42 (2004) 83–94.
[30] S. Haydar, M.A. Ferro-Garcia, J. Rivera-Utrilla, J.P. Joly, Adsorption of *p*-nitrophenol on an activated carbon with different oxidations, Carbon 41 (2003) 387–395.
[31] S. Azizian, Kinetic models of sorption: a theoretical analysis, J. Colloid Interface Sci. 276 (1) (2004) 47–52.
[32] M. Doğan, H. Abak, M. Alkan, Adsorption of methylene blue onto hazelnut shell: kinetics, mechanism and activation parameters, J. Hazard. Mater. 164 (2009) 172–181.
[33] M. Basibuyuk, C.F. Forster, An examination of the adsorption characteristics of a basic dye (Maxilon Red BL-N) on to live activated sludge system, Process Biochem. 38 (2003) 1311–1316.
[34] S. Rengaraj, Y. Kim, C.K. Joo, J. Yi, Removal of copper from aqueous solution by aminated and protonated mesoporous aluminas: kinetics and equilibrium, J. Colloid Interface Sci. 273 (2004) 14–21.
[35] P. Waranusantigul, P. Pokethitiyook, M. Kruatrachue, E.S. Upatham, Kinetics of basic dye (methylene blue) biosorption by giant duckweed (*Spirodella polyrrhiza*), Environ. Pollut. 125 (2003) 385–392.
[36] W.J. Weber, J.C. Morris, Kinetics of adsorption on carbon from solution, J. Sanit. Eng. Div. Am. Soc. Civ. Eng. 89 (1963) 31–59.
[37] V.S. Mane1, I.D. Mall, V.C. Srivastava, Kinetic and equilibrium isotherm studies for the adsorptive removal of Brilliant Green dye from aqueous solution by rice husk ash, J. Environ. Manage. 84 (4) (2007) 390–400.
[38] A. Khenifi, B. Zohra, B. Kahina, H. Houari, D. Zoubir, Removal of 2,4-DCP from wastewater by CTAB/bentonite using one-step and two-step methods: a comparative study, Chem. Eng. J. 146 (2009) 345–354.

[39] D. Kumar, J.P. Gaur, Chemical reaction- and particle diffusion-based kinetic modeling of metal biosorption by a *Phormidium* sp.-dominated cyanobacterial mat, Bioresource Technol. 102 (2011) 633–640.
[40] F.C. Wu, R.L. Tseng, R.S. Juang, Comparisons of porous and adsorption properties of carbons activated by steam and KOH, J. Colloid Interface Sci. 283 (2005) 49–56.
[41] Y.S. Al-Degs, M.I. El-Barghouthi, A.A. Issa, M.A. Khraisheh, G.M. Walker, Sorption of Zn(II), Pb(II) and Co(II) using natural sorbents: equilibrium and kinetic studies, Water Res. 40 (2006) 2645–2658.
[42] F. Wu, R. Tseng, R. Juang, Initial behavior of intraparticle diffusion model used in the description of adsorption kinetics, Chem. Eng. J. 153 (2009) 1–8.
[43] E. Boyd, A.W. Adamson, L.S. Meyers, The exchange adsorption of ions from aqueous solution by organic zeolites. II. Kinetics, J. Am. Chem. Soc. 69 (1947) 2836–2848.
[44] K.V. Kumar, V. Ramamurthi, S. Sivanesan, Modeling the mechanism involved during the sorption of methylene blue onto fly ash, J. Colloid Interface Sci. 284 (2005) 14–21.
[45] M. Sankar, G. Sekaran, S. Sadulla, T. Ramasami, Removal of diazo and triphenylmethane dyes from aqueous solutions through an adsorption process, J. Chem. Technol. Biotechnol. 74 (1999) 337.
[46] V.K. Gupta, A. Mittal, V. Gajbe, J. Mittal, Adsorption of basic fuchsin using waste materials–bottom ash and deoiled soya—as adsorbents, J. Colloid Interface Sci. 319 (2008) 30–39.
[47] W.S. Wan Ngah, A. Kamari, Y.J. Koay, Equilibrium and kinetics studies of adsorption of copper(II) on chitosan and chitosan/PVA beads, Int. J. Biol. Macromol. 34 (2004) 155–161.
[48] A. Kilislioglu, B. Bilgin, Thermodynamic and kinetic investigations of uranium adsorption on amberlite IR-118H resin, J. Appl. Radiat. Isotopes 58 (2) (2003) 155–160.
[49] M. Mahramanlioglu, I. Kizilcikli, I.O. Bicer, Adsorption of fluoride from aqueous solution by acid treated spent bleaching earth, J. Fluorine Chem. 115 (2002) 41–47.
[50] X.E. Shen, X.Q. Shan, D.M. Dong, X.Y. Hua, G. Owens, Kinetics and thermodynamics of sorption of nitroaromatic compounds to as-grown and oxidized multiwalled carbon nanotubes, J. Colloid Interface Sci. 330 (2009) 1–8.
[51] B. von Oepen, W. Kördel, W. Klein, Sorption of nonpolar and polar compounds to soils: processes, measurements and experience with the applicability of the modified OECD-Guideline 106, Chemosphere 22 (1991) 285–304.